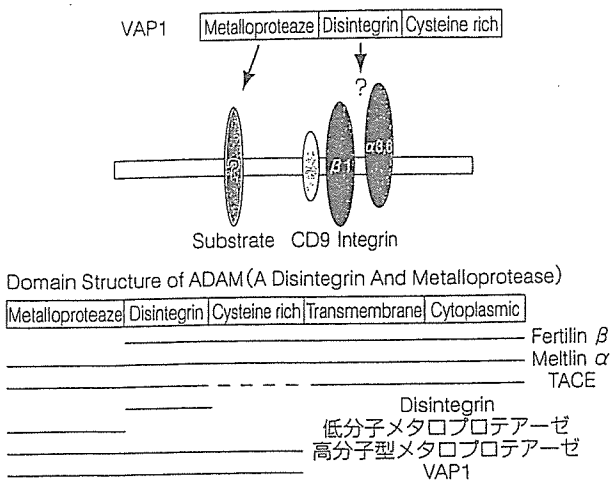


図❹A　血管内皮アポトーシス誘導因子
(Takeda S *et al*, 2006[9]より引用)

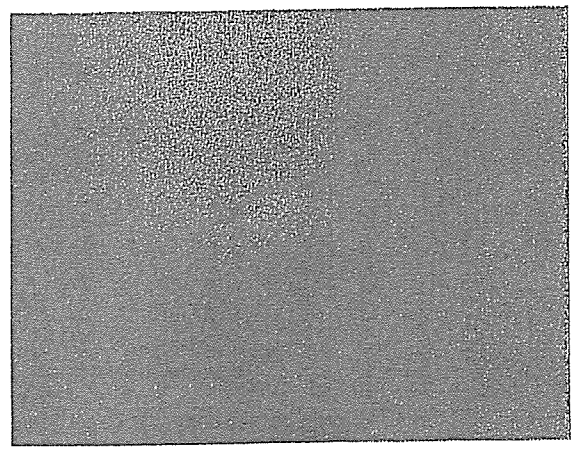

図❹B　蛋白結晶

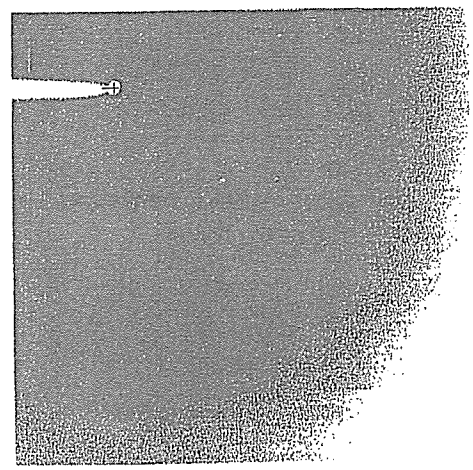

図❹C　X線回折像

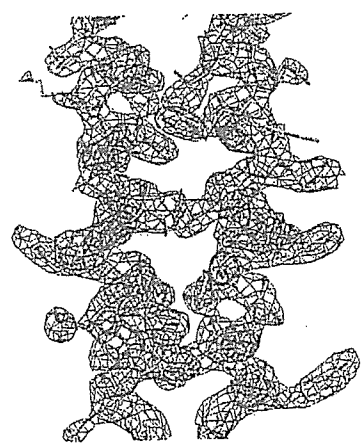

図❺　放射光X線回折像から得られた電子密度図
ヒト心筋トロポニン複合体の電子密度図2.6Å分解能.

TnT（図中黄色）とよばれる3つのドメインからなる．これまでの研究により，TnIは収縮抑制因子，TnCは脱抑制因子，TnTはTnCの脱抑制を弱める因子（$Ca^{2+}$濃度依存性の付加因子）であることが示されている[3]．

TnCはN末端側とC末端側の2つの球状部が$\alpha$ヘリックスで連結された構造をもつ．$Ca^{2+}$濃度にかかわらずC末側球状部はTnIに結合し，TnCをトロポニン分子内につねにつなぎとめている．一方，TnCのN末端側球状部は細胞内$Ca^{2+}$濃度が上昇した場合のみ構造が開き，TnIの第2結合部位（両親媒性$\alpha$ヘリックスH3）を結合する(図中結合部位)．これにより，TnIの調節領域（トロポミオシンをアクチンに結びつけている部分）全体(H3，H4からC-TnIまでを指す)がトロポミオシン/アクチンより解離し，アクチンとミオシンの滑り運動が始まる．

TnCのN末端側球状部に$Ca^{2+}$センシタイザーが結合すると同球状部は開いた構造をとり，TnIの第2結合部位を結合しやすくなる(図❻右側赤のドメイン)．すなわち，TnCによるTnIの脱抑制が起こりやすくなる[4][5]．TnCを介した$Ca^{2+}$感受性の調節薬は心疾患一般に適用できる強心剤として期待がもてる．従来の強心剤は細胞内$Ca^{2+}$イオン濃度を高めて強心作用を誘導するために，細胞に対する負荷（$Ca^{2+}$ overload）が不可避であった．1980年代後半に開発された$Ca^{2+}$センシタイザーと呼ばれた薬剤群（図❻左上）は$Ca^{2+}$イオン濃度—張力関係を

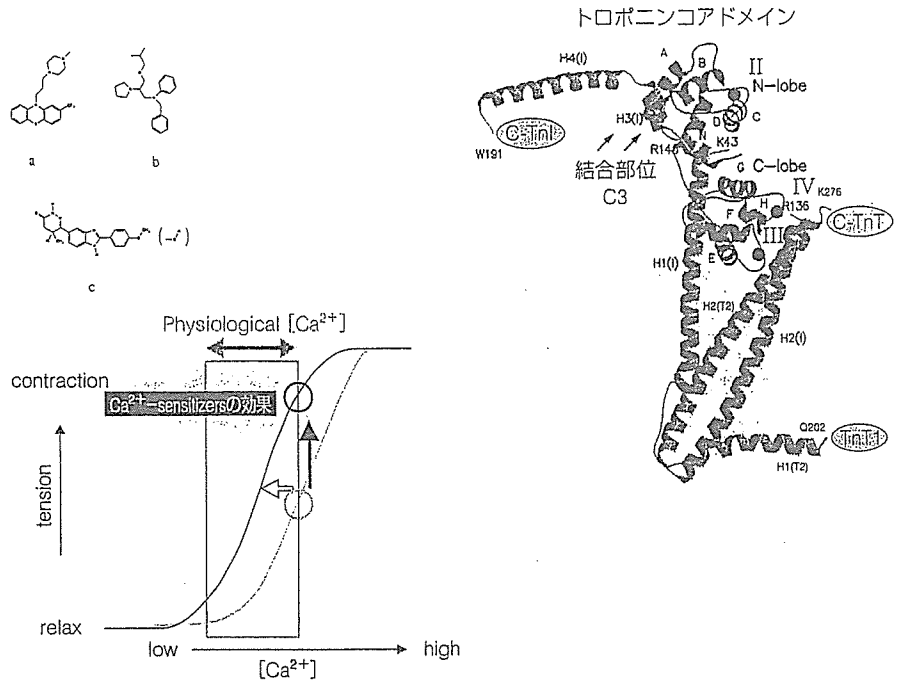


図❻　トロポニンコアドメインの構造と $Ca^{2+}$センシタイザー

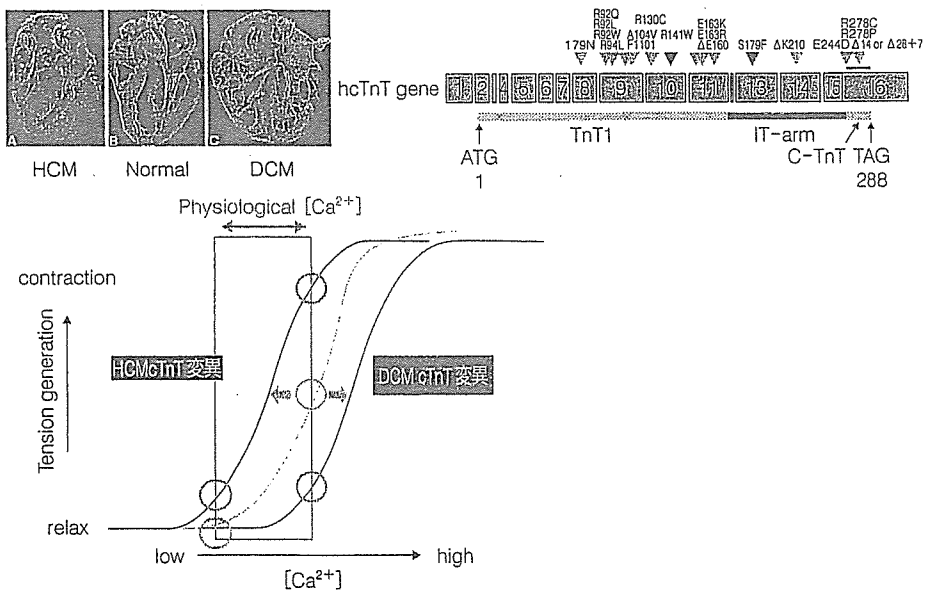


図❼　心筋症におけるトロポニンの遺伝子変異と筋 $Ca^{2+}$感受性

左方にシフトさせることにより(図❻左下)，低い細胞内$Ca^{2+}$イオン濃度で高い収縮力を得ることができる理想的な強心剤ではないかと期待された[6]．しかしながら，これらの薬剤の臨床使用経験から，短期的に心筋収縮力は高まるものの，心不全患者の長期予後の改善に役立つことはなかった．これらの$Ca^{2+}$センシタイザーはphoshodiesteraseの阻害作用もあわせてもっており，細胞内cyclic-AMPの増加によって筋小胞体からの$Ca^{2+}$イオン放出が増加し，ついには$Ca^{2+}$ overloadとなる可能性[7]や，構造が類似したほかの蛋白と相互作用があるなど，

薬剤としての標的特異性が低いことが原因として考えられる．トロポニンを特異的に制御する化合物の設計により，新たな強心剤を開発できる可能性がある．

HCMではトロポニンの遺伝子変異が15%の患者に認められ，その変異による$Ca^{2+}$感受性の亢進が発病に関連すると考えられている．大槻[3]によれば，トロポニンがアクチン/トロポミオシンと直接接触する部分（TnT1，C-TnT，TnI調節領域）に変異が多く認められる（図❼右上）．変異TnTの交換導入をおこなった心筋スキンドファイバーを用いた研究で，$Ca^{2+}$イオン濃度一張力関係の左方シフト，すなわち$Ca^{2+}$感受性の亢進が認められた（図❼下左側グラフ）．HCMにおける変異トロポニンを発現する遺伝子導入マウスを作製することでHCMの発症と個々の遺伝子異常の関連を実証することができる．その際に，白井らが別稿に述べるような放射光小角散乱法は，生体下で収縮蛋白の分子機能を評価することにより，病態解明と治療法の評価に役立つと想像される．TnTの変異による$Ca^{2+}$感受性亢進のメカニズムを原子構造で解明することができれば，構造に基づく薬剤の設計により，HCMを遺伝子変異ごとに特異的に治療する薬剤の設計を期待できる．

2）イオン交換輸送体調節蛋白複合体

$Na^+/H^+$交換輸送体（NHE）の多くは細胞膜に存在して細胞内の$H^+$と細胞外の$Na^+$を交換することで，細胞内のpH調節，$Na^+$とそれに伴う水分量調節に寄与している．膜型NHEの細胞内ドメインに結合する$Ca^{2+}$結合蛋白質の1つ，カルシニューリン様蛋白質CHPがNHEの活性制御に重要である[8]．具体的にはCHPが結合することでNHEが活性化され，細胞内pHを上昇させる（図❸A）．癌細胞の増殖にNHEの活性化による細胞内pHの上昇が関与する．CHP1はあらゆる組織に存在するが，CHP2は癌細胞に特異的に発現する．われわれは癌細胞に特異的に発現するCHP2とNHE複合体の結晶の作製に成功し（図❸B），その結晶構造をX線回折法（図❸C）で決定した．CHP2/NHEペプチド複合体を大量精製した後，EFハンド$Ca^{2+}$部位を$Y^{3+}$イオンで置換することによって結晶化をおこない，SPring-8の放射光を用いて2.8Åの解像度で結晶構造を解明した．その結果，CHP2とNHEがきわめて特異的に強く相互作用する分子機構が明らかになった．構造に基づく機能解析によってCHP2が$Ca^{2+}$センサーではなくNHEのpHセンサーを制御するユニークな機能を有することが明らかになった．創薬的観点から，CHP2/NHE相互作用を阻害する薬剤の設計により新たな癌治療薬の開発が期待できる．

3）血管内皮アポトーシス誘導因子

血管内皮細胞アポトーシス誘導因子（vascular apoptosis inducing protein 1：VAP1）は血管内皮細胞のアポトーシスを誘導して出血を引き起こす蛇毒である[9]．この蛋白の構造解析は新たな血管再生医療法の開発に道をひらく可能性がある．またVAP1のアミノ酸配列はヒトADAM（a disintegrin and metalloprotease）ファミリー蛋白と高い相同性を有しており[9]，それらの分子機構の解明の端緒となる可能性がある（図❹A）．たとえば，TNF-$\alpha$ converting enzyme（TACE：ADAM17）はADAMファミリー蛋白に属する蛋白の1つで，膜結合型シグナル因子（TNF-$\alpha$など）の切断遊離に関与する[10]．TNF-$\alpha$も細胞のアポトーシスを誘導する．ほかのADAM蛋白と同様にプロテアーゼドメイン，disintegrin，システインリッチドメインからなるVAP1の結晶化に成功し（図❹B），放射光X線回折法で構造を2.5Å分解能で解明した（図❹C）[9]．サイトカインなどの膜結合型シグナル因子の切断遊離機構（ectodomain shedding）の説明にも演繹できる構造解析結果を得た[9]．

## おわりに

21世紀の医療の社会的課題として提唱されているテーラーメード医療の達成には，標的となる蛋白の構造を患者ごとに確定し（分子診断），最適な薬剤の構造を選択し（分子治療），薬剤と生体蛋白の相互作用を分子レベルで観察する（分子評価）などの医療基盤技術の育成が求められる．ナノレベルイメージングプロジェクトでは，蛋白分子の構造と機能の解析を通じて，テーラーメード医療実現のための基盤技術の形成に貢献している．

謝辞　本稿編集に協力していただいた東本弘子女史に感謝し

ます.

## 文　献


1) Drucker BJ *et al* : Effects of a selective inhibitor of the Abl tyrosine kinase on the growth of Bcr-Abl positive cells. *Nature Medicine* 2 : 561-566, 1996
2) Branden Carl *et al* : *Introduction to Protein Structure*. Garland Publishing Inc. New York, 1999, pp. 373-383
3) 大槻磐男：筋収縮カルシウム受容調節の分子機構と遺伝性機能障害. 日本薬理学雑誌 118 : 147-158, 2001
4) Takeda S *et al* : Structure of the core domain of human cardiac troponin in the $Ca^{2+}$saturated form. *Nature* 424 : 35-41, 2003
5) 前田雄一郎ほか：トロポニンの結晶構造とカルシウム調節のメカニズム. タンパク質　核酸　酵素 48 : 500-512, 2003
6) Lee JA *et al* : Effects of pimobendan, a novel inotropic agent on intracellular calcium and tension in isolated ferret ventricular muscle. *Clinical Science* 76 : 609-618, 1989
7) Nieminen MS *et al* : Executive summary of the guidelines on the diagnosis and treatment of acute heart failure : the Task Force on Acute Heart Failure of the European society of Cardiology. *Eur Heart J* 26 : 384-416, 2005
8) Ammar YB *et al* : Crystal structure of CHP2 complexed with NHE1-cytosolic region and an implication for pH regulation. *EMBO J* 25 : 2315-2325, 2006
9) Takeda S *et al* : Crystal structure of VAP1, a snake venom metalloproteinase/disintegrin/cysteine-rich protein. *EMBO J* : 2006 (in press)
10) Black RA *et al* : A metalloproteinase disintegrin that releases tumour necrosis factor-alpha from cells. *Nature* 385 : 729-733, 1997



**MORI Hidezo**

国立循環器病センター研究所心臓生理部長
もり・ひでぞう
慶應義塾大学医学部卒業.
慶應義塾大学大学院医学研究科修了.
慶應義塾大学医学部・助手，国立埼玉病院循環器科医長，東海大学医学部講師・助教授を経て，国立循環器病センター研究所心臓生理部長（2000年10月）.
大阪大学大学院医学系研究科招聘教授，東海大学医学部非常勤教授を兼務（2004年4月）.
研究テーマ：微小循環，再生医療，ナノメディシン.

# ナノレベルイメージングによる分子構造と機能の解析

盛　英三[1]　望月直樹[1]　武田壮一[1]
井上裕康[2]　中村　俊[3]　土屋利江[4]

## Nano-level imaging for analyzing protein structure and function

[1]Hidezo Mori, [1]Naoki Mochizuki, [1]Soichi Takeda,
[2]Hiroyasu Inoue, [3]Shun Nakamura, [4]Toshie Tsuchiya
[1]National Cardiovascular Center Research Institute
[2]Faculty of Human Life and Environment, Nara Women's University
[3]National Center of Neurology and Psychiatry
[4]National Institute of Health Sciences

**Abstract**

The present manuscript outlines the nano-level imaging project, which is under promotion by the three national research institutes and supported by a research grant from the Ministry of Health, Labor and Welfare (nano-001). This research project targets collecting fundamental information regarding comprehensive understanding of cardiovascular, neurological and the other disorders, developing new diagnostic and therapeutic methods by visualizing protein structure and function in atomic (sub-nano level) or molecular (nano-level) resolution. The results of the current projects will be extended into drug design, clinical diagnostic technology and medical materials in near future.

**Key words**: nano-technology, structural biology, drug design, protein crystallography, tailor-made medicine

## はじめに

21世紀の医療の社会的課題として提唱されているテーラーメード医療の達成には，標的となる蛋白の構造を患者ごとに確定し(分子診断)，最適な薬剤の構造を選択し(分子治療)，薬剤と生体蛋白の相互作用を分子レベルで観察する(分子評価)などの医療基盤技術の育成が求められる．ナノレベルイメージングプロジェクトでは，蛋白分子の構造と機能の解析を通じてテーラーメード医療実現のための基盤技術の形成を目指している．

本稿では蛋白構造イメージングを中心に概説する．

## 1. 創薬に貢献した分子構造イメージング

近年，放射光を用いたX線回折法の発達により原子レベルの解像度で蛋白結晶の構造を決定できるようになった．構造に基づく薬剤設計の具体的な成功例として，AIDS治療薬(HIVプロ

[1]国立循環器病センター研究所　[2]奈良女子大学生活環境学部　[3]国立精神神経センター　[4]国立医薬品食品衛生研究所

0047-1852/06/¥40/頁/JCLS

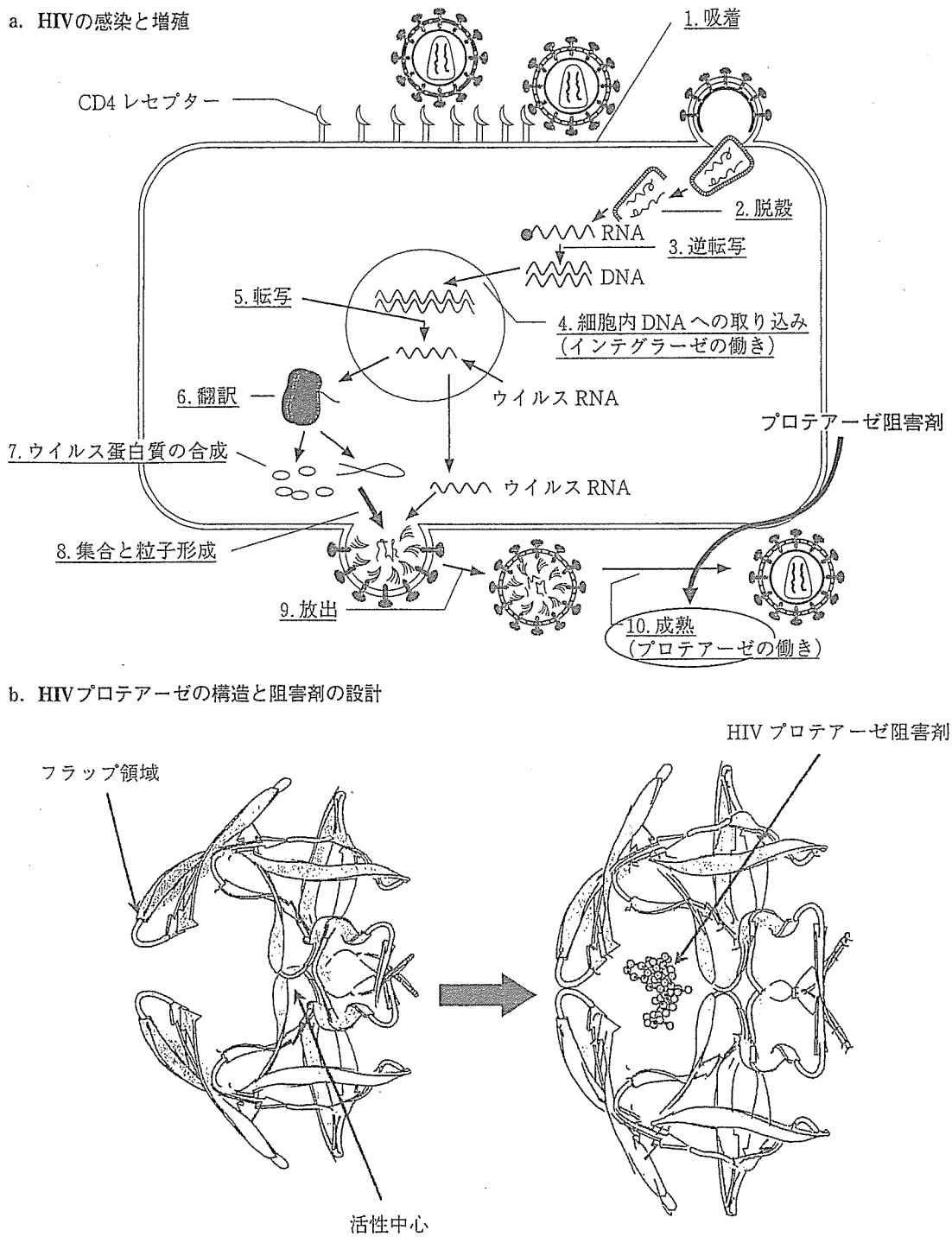


図1 AIDSウイルスの増殖過程と蛋白構造に基づくHIVプロテアーゼ阻害薬の作用機構

テアーゼ阻害薬), 白血病治療薬(グリベック)について以下に述べる.

AIDSウイルス, HIVは活性化外殻蛋白gp120によりCD4陽性Tリンパ球に感染し, 自己増殖をする. その際自己由来のプロテアーゼによって前駆体蛋白から活性化外殻蛋白を得る(図1-a). このHIVプロテアーゼの構造に基づいて設計され, その活性中心を選択的に阻害する目的で設計された薬剤がHIVプロテアーゼ阻害薬である(図1-b). 本剤はAIDSの発症を遅らせることに貢献した[1].

慢性骨髄性白血病ではフィラデルフィア染色

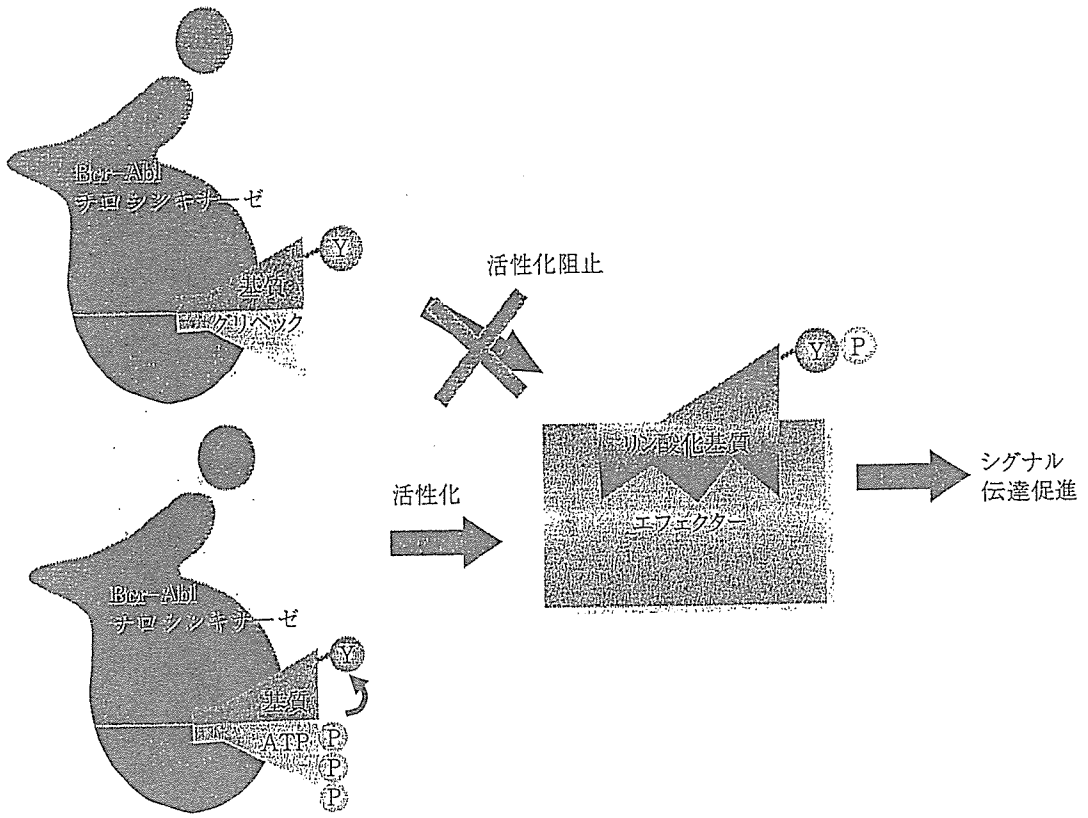


図2 慢性白血病治療薬(グリベック)の蛋白構造に基づく作用機構

体に由来するBcr-Ablチロシンキナーゼが恒常的な増殖シグナル伝達系の活性化を通じて慢性骨髄性白血病発症の原因になると考えられている．同酵素はATPと基質に結合し，ATPから切り離したリン酸基で基質のチロシン残基をリン酸化する．グリベックはBcr-AblチロシンキナーゼのATP結合部位の詳細な構造に基づいて設計され，基質のチロシンリン酸化を構造特異的に阻害して白血病化を防ぐ(図2)[2]．

このような構造に基づいて薬剤設計を行うことで標的蛋白との結合の特異性を高め，副作用を減少させることを期待できる．

## 2. ヒト心筋トロポニンの構造解析とそれに基づく創薬の可能性

心筋収縮を調節する心筋トロポニンの中核部分(コアドメイン)の構造は分担研究者である武田と理化学研究所の前田らによって解析され，Nature誌に報告された(Vol 424, 2003)[3]．前田らの総説[4]に基づき，トロポニンの筋収縮調節メカニズムについて述べる．

筋収縮はアクチンとミオシンの滑り運動による．アクチンフィラメントはアクチン，トロポニン，トロポミオシンを含む複合体であり，それらの3分子は7：1：1の存在比をもつ．トロポニンの存在下でアクチンとミオシンはカルシウムイオン濃度に応じた収縮と弛緩を行う．

図3に心筋トロポニンのコアドメインの構造を示す．トロポニンはTnC，TnI，TnTと呼ばれる3つのポリペプチド鎖からなる．これまでの研究により，TnIは収縮抑制因子，TnCは脱抑制因子，TnTはTnCの脱抑制を弱める因子(カルシウム濃度依存性の付加因子)であることが示されている[5]．

トロポニンのコアドメインは更に調節頭部とITアームの2つのサブドメインに分かれる．調節頭部はカルシウムイオンとの結合を通じてトロポニンの構造変化とそれに基づくアクチンとミオシンの滑り運動に対するスイッチの役割を果たす．ITアームは剛性を有するコイルドコイ

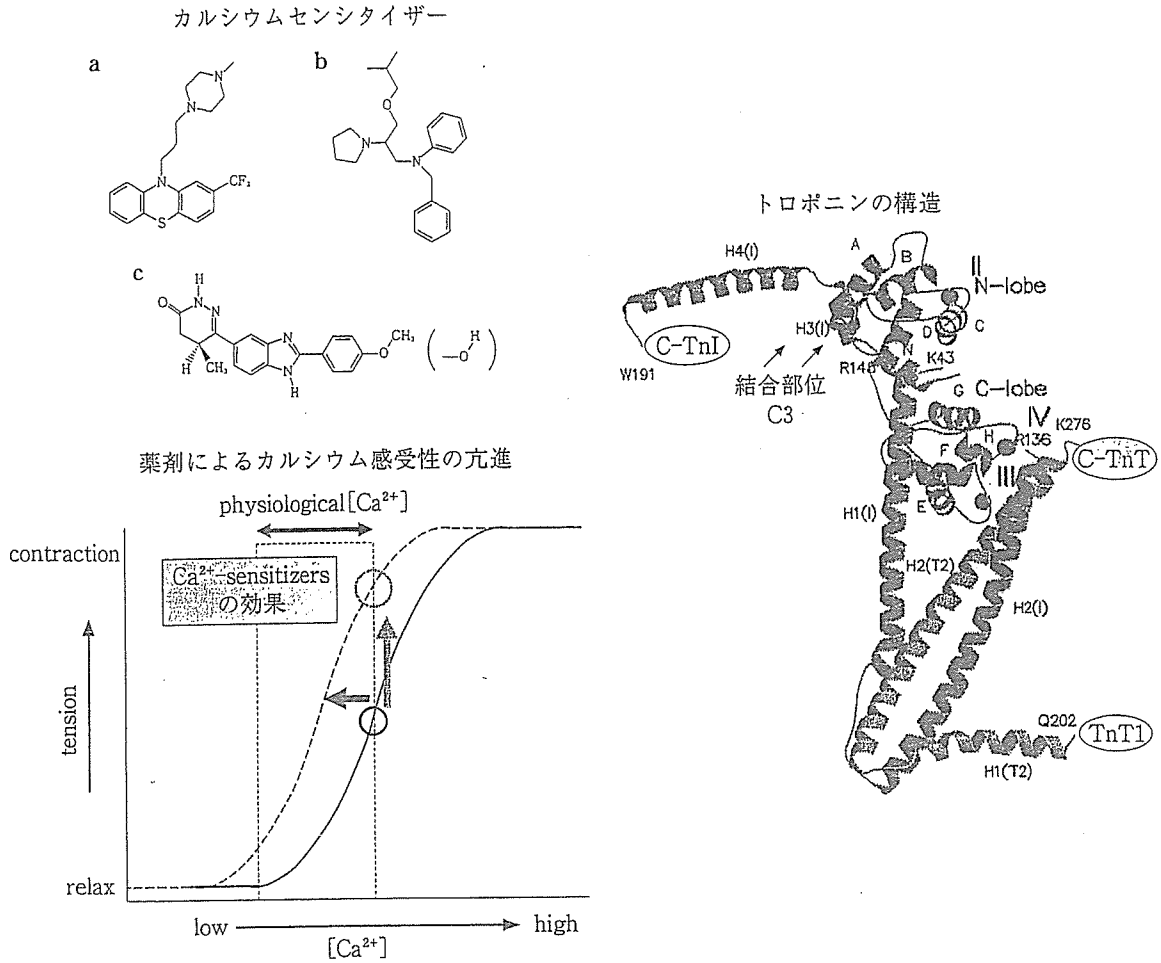


図3 トロポニンコアドメインの構造(文献[3]より改変引用)

ル構造からなる．TnCはN末端側とC末端側の2つの球状部がαヘリックスで連結された構造をもつ．カルシウム濃度にかかわらずC末側球状部はTnIに結合し，TnCをトロポニン分子内に常につなぎとめている．一方，TnCのN末端側球状部は細胞内カルシウム濃度が上昇した場合のみ構造が開き，TnIの第二結合部位(両親媒性αヘリックスH3)を結合する．これにより，TnIの調節領域全体がトロポミオシン/アクチンより解離し，アクチンとミオシンの滑り運動が始まる．

TnCのN末端側球状部にカルシウムセンシタイザーが結合すると，同球状部は開いた構造をとりTnIの第二結合部位を結合しやすくなる．すなわち，TnCによるTnIの脱抑制が起こりやすくなる．前述のようにTnTはTnCの脱抑制作用にカルシウム濃度依存性を付加することができるので，TnCとTnTの制御を組み合わせることで段階的な筋収縮の増強を実現できるかもしれない．近年循環器領域では血管作動性薬剤で優れた新薬が数多く開発されてきたが，ジギタリス以来，これを超える強心剤が生まれていない．従来の強心剤は細胞内カルシウムイオン濃度を高めて強心作用を誘導するために，細胞に対する負荷(カルシウムoverload)が不可避であった．1980年代後半に開発されたカルシウムセンシタイザーと呼ばれた薬剤群はカルシウムイオン濃度-張力関係を左方にシフトさせることにより，低い細胞内カルシウムイオン濃度で高い収縮力を得ることができる理想的な強心剤ではないかと期待された[6]．しかしながら，これらの薬剤の臨床使用経験から，短期的に心筋収縮力は高まるものの，心不全患者の長期予後の改善に役立つことはなかった．これらのカ

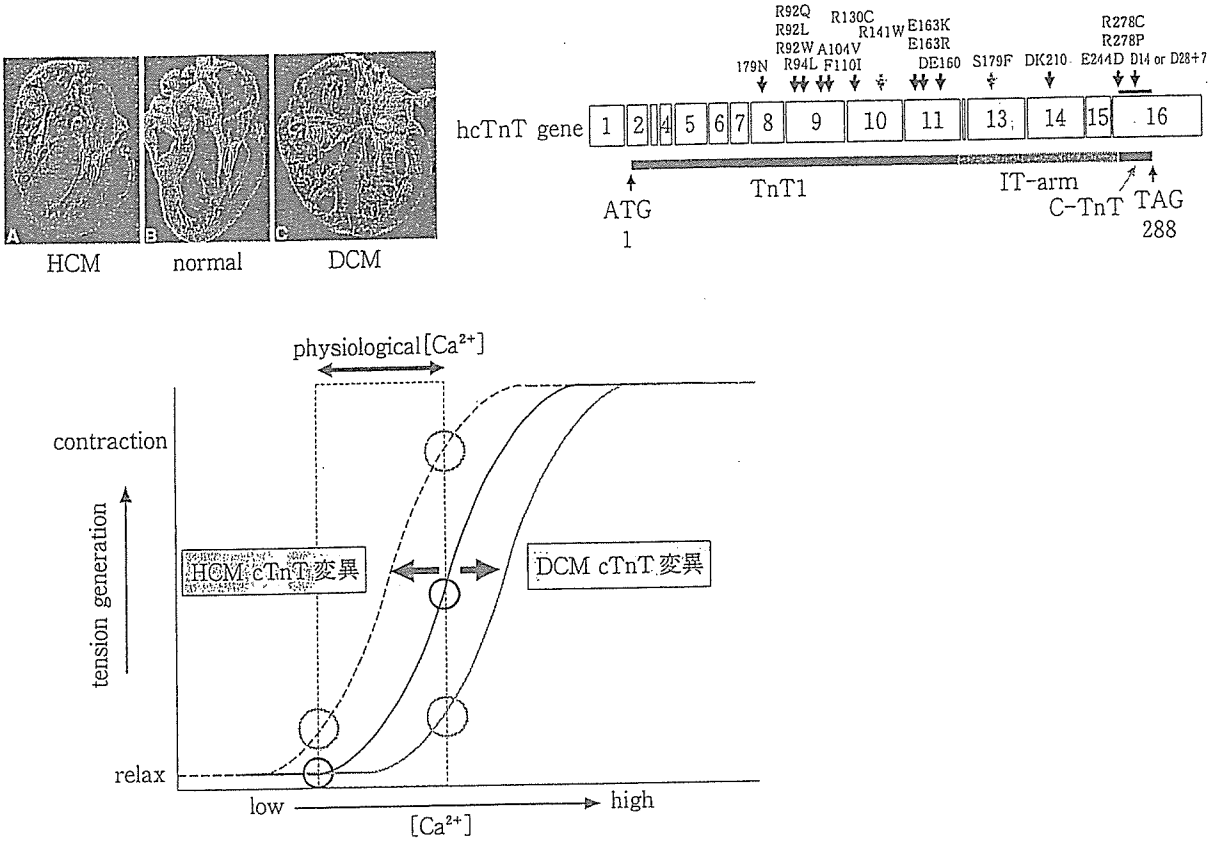


図4 心筋症におけるトロポニンの遺伝子変異と筋カルシウム感受性
心筋症の遺伝子変異はTnT1，C-TnTに多く，筋カルシウム感受性を修飾する．

ルシウムセンシタイザーはphoshodiesteraseの阻害作用も併せてもっており，細胞内cyclic-AMPの増加によって筋小胞体からのカルシウムイオン放出が増加し，ついにはカルシウムoverloadとなる可能性や[7]，構造が類似した他の蛋白と相互作用があるなど，薬剤としての標的特異性が低いことが原因として考えられる．拡張型心筋症例では，少なくとも一部の症例でカルシウム感受性の低下と収縮不全の関連が示唆されている．これらの事実はTnCやTnTを特異的に制御する化合物の設計により，新たな強心剤の開発の可能性を示している．

一方，肥大型心筋症(HCM)ではトロポニンの遺伝子変異によりカルシウム感受性が亢進することが発病に関連する可能性が示唆されている．同患者の遺伝子解析によると，約15％の患者にTnTの遺伝子変異が認められる．大槻らによれば[5]トロポニンがアクチン/トロポミオシンと直接接触する部分(TnT1，C-TnT，TnI調節領域)に変異が多く認められ，コアドメインには変異は少ないという(図4)．変異TnTの交換導入を行った心筋スキンドファイバーを用いた研究で，カルシウムイオン濃度-張力関係の左方シフト，すなわちカルシウム感受性の亢進が認められた．この結果からTnTの変異により，カルシウム感受性が亢進し，収縮増加と弛緩不全という肥大型心筋症に特有の症状が発症するという有力な仮説が生まれる．TnTの変異によるカルシウム感受性亢進のメカニズムを原子構造で解明すると，肥大型心筋症に特異的に作用する薬剤の設計を期待できる．原因となる遺伝子変異ごとに構造が異なる薬剤設計が求められる可能性もある．言い換えれば，心筋トロポニンの変異に基づく肥大型心筋症の治療法の開発はテーラーメード医療のモデルケースとなる可能性がある．

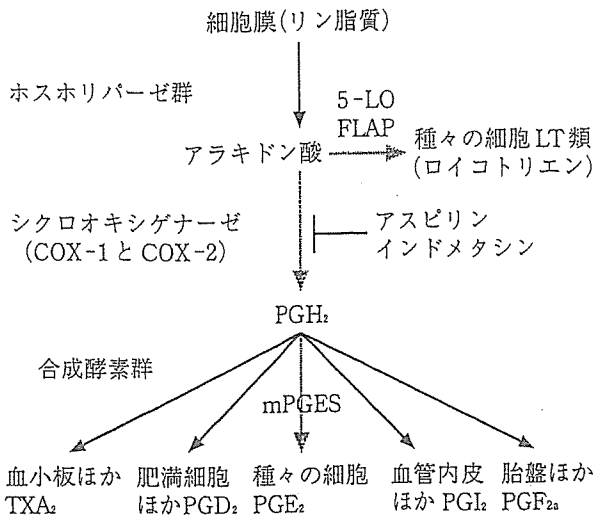


図5 プロスタグランジン産生系

## 3. 創薬の標的として注目されているプロスタグランジン合成酵素群の構造解析

シクロオキシゲナーゼ(COX)はプロスタグランジン(PG)を生合成する律速酵素として知られている(図5)2種類のアイソザイムが存在する．COX-1はconstitutive enzymeと呼ばれ，ほとんどの細胞で常時発現しており，生体の安定性を維持する役割を果たす．一方，COX-2はinducible enzymeとして，単球，線維芽細胞，滑膜細胞などの炎症にかかわる細胞で発現し，炎症性サイトカインなどによって誘導される．従来の非ステロイド系抗炎症剤は，COX-1とCOX-2の両方を阻害するために炎症巣のPGだけでなく，胃粘膜や腎でのPG(特に$PGE_2$)産生を抑制し胃や腎の副作用を合併する．そこで，炎症に深く関与していると考えられるCOX-2だけを選択的に阻害する薬剤の開発が進められてきた．このようにして開発されたCOX-2阻害薬は胃潰瘍を起こしにくい鎮痛剤として好んで投薬されていた．しかしながら，2004年末，米政府は，これらのCOX-2選択的阻害薬の3剤を心筋梗塞や脳梗塞の危険性を高める恐れがあるとして，心臓病患者への処方や多量の長期使用を避けるよう勧告した．COX-2の下流に位置するプロスタサイクリン合成酵素の作用も抑制するために，同酵素に由来する抗血栓性作用や血流増加作用が損なわれることが原因ではないかと考えられている[8]．図5に示したようにCOX-2の下流には多くの合成酵素があってそれぞれの作用を有する蛋白を合成している．個々の合成酵素を選択的に阻害する薬剤の開発が次世代の創薬の標的として注目される．$PGE_2$の産生にかかわるmPGESを阻害する薬物の開発は血管内血栓形成を伴わない理想的な抗炎症剤となる可能性がある．$TXA_2$産生を阻害する薬剤の開発は血管内血栓形成の予防，局所血流増加作用を通じて脳梗塞，心筋梗塞の予防薬や治療薬として期待できる．$PGI_2$は既に難病といわれた原発性肺高血圧症の治療に有効であることが知られている．PG関連薬剤の開発は構造に基づく創薬の最大の標的の一つになっており，ナノメディシンプロジェクトでも複数の関連酵素の構造解析に取り組んでいる．

## 4. ナノメディシンプロジェクトのそのほかの研究

本プロジェクトでは分子構造イメージングに関連して上記のほかに，細胞内イオン環境や，血管新生にかかわる蛋白など幾つかの蛋白構造についても研究を進めている(国立循環器病センター研究所)．国立精神神経センターではin-silicoスクリーニング法によるParkinson病の治療薬探索に蛋白構造情報を応用する研究を進めている．国立医薬品食品衛生研究所では原子間力顕微鏡を用いて蛋白表面の詳細な構造を解析することなどを通じて，医用材料作成に向けた応用研究に取り組んでいる．

一方，分子機能イメージングの領域では，国立循環器病センターの望月らが増殖因子(EGF)刺激に伴うRas分子の活性化をFRET法で可視化できることをNature誌に報告した[9]．ナノメディシンプロジェクト開始後も血管内皮の走化運動にかかわるRap1蛋白の可視化に関する研究などにFRET法による分子イメージングを展開している．国立精神神経センターの研究グループでは分子機能イメージング技術を応用してシナプス機能，プリオン蛋白質の機能の評価に

取り組みProc Natl Acad Sciなどの雑誌に研究成果を報告している[10].

## おわりに

本ナノメディシンプロジェクトでは循環器治療の中核施設である国立循環器病センター内に構造生物学ラボを立ち上げ，分子特異的な治療薬の開発を目指している．ナノDDS技術や分子機能イメージング技術に関する研究を併せて推進することで，特異的分子治療薬の分子輸送技術開発と他の分子との相互作用の可視化技術を推進することが可能となる．これにより，分子診断・分子治療・分子評価を包含するテーラーメード医療の基盤形成に貢献したい．

謝辞　本原稿の執筆内容は本研究グループの成果を元にしております．国立循環器病センター研究所若林繁夫分子生理部長およびユーセフ・ベン・アマー同研究員，増田道隆循環器形態部室長，柴田洋之心臓生理部同室員，五十嵐智子同研究員，松原孝宜同研究員，大阪大学月原富武教授，理化学研究所宮野雅司主任研究員に感謝いたします．また，本原稿編集と英文作成に協力していただいた東本弘子女史，松尾千重女史に感謝します．

## 文献

1) Patick AK, et al: Activities of the human immunodeficiency virus type 1(HIV-1) protease inhibitor nelfinavir mesylate in combination with reverse transcriptase and protease inhibitors against acute HIV-1 infection in vitro. Antimicrob Agents Chemother 41: 2159-2164, 1997.
2) Drucker BJ, et al: Effects of a selective inhibitor of the Abl tyrosine kinase on the growth of Bcr-Abl positive cells. Nat Med 2: 561-566, 1996.
3) Takeda S, et al: Structure of the core domain of human cardiac troponin in the $Ca^{2+}$ saturated form. Nature 424: 35-41, 2003.
4) 前田雄一郎ほか：トロポニンの結晶構造とカルシウム調節のメカニズム．蛋白質核酸酵素 48: 500-512, 2003.
5) 大槻磐男：筋収縮カルシウム受容調節の分子機構と遺伝性機能障害．日薬理誌 118: 147-158, 2001.
6) Lee JA, et al: Effects of pimobendan, a novel inotropic agent on intracellular calcium and tension in isolated ferret ventricular muscle. Clin Sci 76: 609-618, 1989.
7) Nieminen MS, et al: Executive summary of the guidelines on the diagnosis and treatment of acute heart failure: The task force on acute heart failure of the European society of cardiology. Eur Heart J 26: 384-416, 2005.
8) Mukherjee D, et al: Risk of cardiovascular events associated with selective cox-2 inhibitors. JAMA 286: 954-959, 2001.
9) Mochizuki N, et al: Spatio-temporal images of growth-factor-induced activation of Ras and Rap1. Nature 411: 1065-1068, 2001.
10) Itami C, et al: Brain-derived neurotrophic factor-dependent unmasking of silent synapses in developing mouse barrel cortex. Proc Natl Acad Sci USA 100: 13069-13074, 2003.

Acta Crystallographica Section F
Structural Biology and Crystallization Communications
ISSN 1744-3091

Youssef Ben Ammar,[a] Soichi Takeda,[b] Mitsuaki Sugawara,[c] Masashi Miyano,[c] Hidezo Mori[b] and Shigeo Wakabayashi[a]*

[a]Department of Molecular Physiology, National Cardiovascular Center Research Institute, Fujishiro-dai 5-7-1, Suita, Osaka 565-8565, Japan, [b]Department of Cardiac Physiology, National Cardiovascular Center Research Institute, Fujishiro-dai 5-7-1, Suita, Osaka 565-8565, Japan, and [c]Structural Biophysics Laboratory, RIKEN Harima Institute at SPring-8, Kouto, Mikazuki, Sayo, Hyogo 679-5148, Japan

Correspondence e-mail: wak@ri.ncvc.go.jp

Received 18 August 2005
Accepted 27 September 2005
Online 30 September 2005

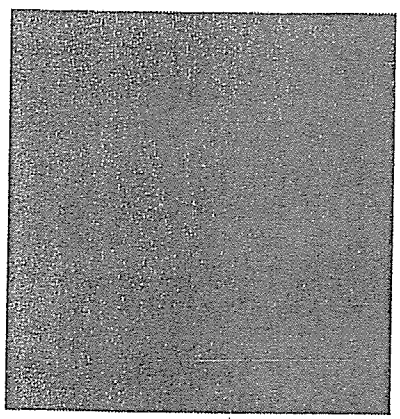



# Crystallization and preliminary crystallographic analysis of the human calcineurin homologous protein CHP2 bound to the cytoplasmic region of the $Na^+/H^+$ exchanger NHE1

Calcineurin homologous protein (CHP) is a $Ca^{2+}$-binding protein that directly interacts with and regulates the activity of all plasma-membrane $Na^+/H^+$-exchanger (NHE) family members. In contrast to the ubiquitous isoform CHP1, CHP2 is highly expressed in cancer cells. To understand the regulatory mechanism of NHE1 by CHP2, the complex CHP2–NHE1 (amino acids 503–545) has been crystallized by the sitting-drop vapour-diffusion method using PEG 3350 as precipitant. The crystals diffract to 2.7 Å and belong to a tetragonal space group, with unit-cell parameters $a = b = 49.96$, $c = 103.20$ Å.

## 1. Introduction

The $Na^+/H^+$ exchangers (NHEs) are electroneutral transporters that catalyze the countertransport of $Na^+$ and $H^+$ through the plasma membrane and other intracellular organellar membranes in various animal species (Wakabayashi *et al.*, 1997; Orlowski & Grinstein, 2004). Nine different NHE isoforms (NHE1–NHE9) have been identified in mammalian tissues. Although they have been shown to exhibit similar membrane topology, these isoforms are thought to play different roles in various tissues (Counillon & Pouysségur, 2000; Orlowski & Grinstein, 2004). The isoform NHE1 is ubiquitously expressed in all tissues and cell types and plays a major role in maintaining intracellular pH and cell-volume homoeostasis (Putney *et al.*, 2002). The activity of NHE1 is controlled by various extrinsic factors, including growth factors, hormones and mechanical stimuli (Wakabayashi *et al.*, 1997; Counillon & Pouysségur, 2000; Orlowski & Grinstein, 2004). NHE1 is regulated by a variety of signalling molecules including calcineurin B homologous protein (CHP; Lin & Barber, 1996; Pang *et al.*, 2001) and $Ca^{2+}$/calmodulin (Bertrand *et al.*, 1994; Wakabayashi *et al.*, 1994). Despite intensive studies on NHE1 and its regulation, structural information is extremely limited, especially for the cytoplasmic C-terminal domain which contains most of the binding domains for the regulatory proteins.

CHP was initially identified as a protein (p22) involved in vesicular transport (Barroso *et al.*, 1996) and also as a molecule that interacts with NHE (Lin & Barber, 1996). CHP has also been reported to be involved in various cell functions, such as inhibition of calcineurin phosphatase activity (Lin *et al.*, 1999) and interaction with microtubules (Timm *et al.*, 1999), DRAK2 (death-associated protein kinase-related apoptosis-inducing protein kinase 2; Matsumoto *et al.*, 2001) and KIF1B$\beta$2 (kinesin family 1Bb2; Nakamura *et al.*, 2002). We have previously reported that CHP is an essential cofactor for supporting the physiological activity of the $Na^+/H^+$ exchanger by interacting with its juxtamembrane cytoplasmic domain (Pang *et al.*, 2001). Furthermore, we demonstrated that in contrast to the ubiquitous CHP1 isoform, CHP2 (61% amino-acid identity with CHP1) is highly expressed in malignantly transformed cells and may be involved in maintaining the high intracellular pH ($pH_i$) in cancer cells (Pang *et al.*, 2002). NHE1 mutants lacking the CHP-binding region (amino acids 515–530) exhibited low exchange activity (5–10% of the wild-type level; Pang *et al.*, 2001), suggesting that this region is essential for normal exchange activity of NHE1. This region with bound CHP would therefore function as a key structure maintaining the physiologically active conformation of NHE1 (Pang *et al.*, 2001).

Consequently, more detailed structural information including the crystal structure of CHP complexed with its binding domain is of great importance to reveal the mechanism by which CHP is involved in this important regulation pathway of NHE1.

Here, we report the first crystallization and preliminary crystallographic studies of the human CHP2 complexed with the C-terminal cytoplasmic region (amino acids 503–545) of NHE1. Hereafter, the protein complex is referred to as CHP2–NHE1-peptide.

## 2. Materials and methods

### 2.1. Protein expression and purification

Human CHP2 cDNA (GenBank accession No. AF146019) corresponding to amino-acid residues 1–196 cloned into pET11 vector (Novagen) as a fusion protein with a C-terminal $His_6$ tag was co-expressed in *Escherichia coli* (BL21-Star; Invitrogen) with the human cDNA encoding the cytoplasmic binding-domain region of NHE1 peptide cloned into pET24 vector (Novagen). Six histidine residues were inserted after Lys196 of CHP2, while a stop codon was incorporated just after the sequence coding for the NHE1 peptide to eliminate the $His_6$ tag from the vector. Using this coexpression system, as also described previously for CHP1 (Pang *et al.*, 2004), we were able to obtain CHP2 in a complex form with its binding domain of NHE1. Cells were cultured in 2×YT medium containing 100 μg ml$^{-1}$ ampicillin and 100 μg ml$^{-1}$ kanamycin at 310 K. At an optical density of 0.6 at 600 nm, protein expression was induced by the addition of IPTG to a final concentration of 1 m*M* and cells were grown overnight at 291 K. The cells were harvested and resuspended in PBS buffer containing 1 m*M* phenylmethylsulfonyl fluoride (PMSF) and disrupted by sonication at 277 K. After centrifugation at 277 K, the supernatant containing the complex CHP2–NHE1-peptide was applied onto an Ni–NTA agarose affinity column (Invitrogen) equilibrated with PBS buffer. The column was washed with buffer *A* (20 m*M* sodium phosphate, 500 m*M* NaCl and 2 *M* KCl pH 6.0), buffer *B* (20 m*M* sodium phosphate and 500 m*M* NaCl pH 4.7) and then buffer *C* (20 m*M* sodium phosphate and 500 m*M* NaCl pH 6.0). The adsorbed protein complex was eluted with buffer *C* containing 500 m*M* imidazole, dialyzed overnight against buffer *D* (20 m*M* Tris–HCl pH 8.5) and further purified using a DEAE-Sepharose column (HiTrap DEAE FF 5 ml; Amersham Biosciences) eluted with a gradient from 0 to 1 *M* NaCl in 20 m*M* Tris–HCl buffer pH 8.5. A final purification step was carried out using gel-filtration chromatography (Superdex 200; Amersham Bioscience). The gel-filtration column was eluted with a buffer solution containing 100 m*M* NaCl and 20 m*M* Tris–HCl pH 7.5. The fraction containing CHP2–NHE1-peptide was pooled, dialyzed against 20 m*M* Tris–HCl pH 7.5, concentrated (20–25 mg ml$^{-1}$) using Amicon Ultra (Millipore) and subjected to crystallization without removing the $His_6$ tag.

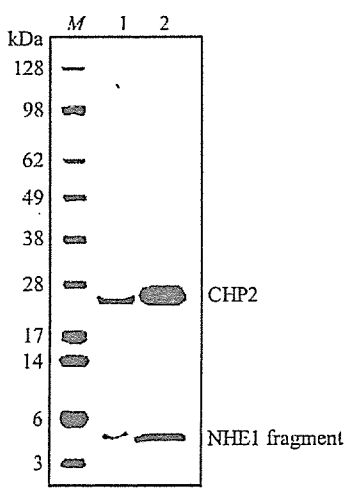


**Figure 1**
Polyacrylamide gel-electrophoresis pattern of the complex CHP2–NHE1-peptide. Crystals were collected and washed with the cryoprotectant solution. Collected crystals and 10 μg of the purified complex were applied to 4–12% gradient gel for lanes 1 and 2, respectively. Proteins were stained with Coomassie Brilliant Blue.

### 2.2. Crystallization

Preliminary screening of crystallization conditions was performed using various commercial kits (Hampton Research Crystal Screen kits, Emerald BioSystems Screen kits, Sigma–Aldrich Crystallization kits) and carried out using the sitting-drop vapour-diffusion method at 293, 287 and 277 K. 1 μl aliquots of protein-complex solution (20–25 mg ml$^{-1}$) were mixed with 1 μl reservoir solution to form the droplet, which was equilibrated against 100 μl reservoir solution. The initial screening, involving about 1440 individual trials, was unsuccessful. Additives from Hampton Research were used together with the above screening kits in a second trial involving about 4320 individual trials and very small and thin needle-shape crystals were finally obtained with a crystallization solution containing 200 m*M* ammonium acetate, 100 m*M* Bis-Tris pH 5.5, 25%(*w*/*v*) polyethylene glycol 3350 (PEG 3350) and 5 m*M* yttrium chloride as an additive at 277 K. Refinement of the crystallization conditions to 200 m*M* ammonium acetate, 100 m*M* Bis-Tris pH 5.5, 25%(*w*/*v*) PEG 3350 and 10 m*M* yttrium chloride at 293 K improved the size of the crystals. The resultant crystals are mostly in clusters, with the occasional appearance of single crystals. Single crystals or dissected parts from the clusters were used for data collection.

### 2.3. Crystallographic data collection

Prior to data collection, single crystals were soaked in a solution containing 200 m*M* ammonium acetate, 100 m*M* Bis-Tris pH 5.5, 35%(*w*/*v*) PEG 3350 and 10 m*M* yttrium chloride and flash-frozen under a nitrogen flow at 100 K. The crystals were evaluated in-house with Cu $K\alpha$ radiation ($\lambda$ = 1.5418 Å) generated by an RA-Micro 7 rotating-anode X-ray generator with R-AXIS VII imaging-plate detector (Rigaku). High-resolution data sets were collected using an

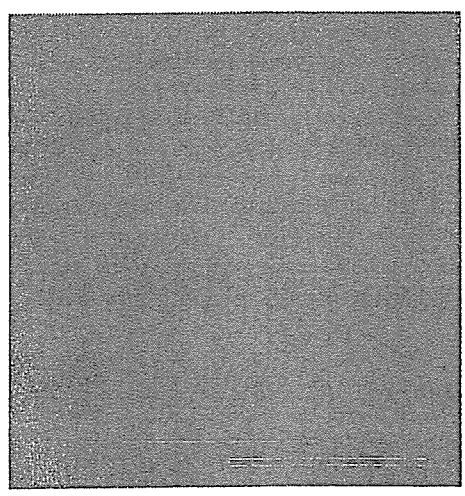

**Figure 2**
Crystal of human CHP2–NHE1-peptide as grown by the sitting-drop method. The scale bar indicates 0.1 mm.

Table 1
Data-collection statistics.

Values in parentheses are for the highest resolution shell (2.8–2.7 Å).

| | |
|---|---|
| X-ray source | SPring-8 BL41XU |
| Space group | $P4_1$ or $P4_3$ |
| Unit-cell parameters (Å, °) | $a = b = 49.96$, $c = 103.20$, $\alpha = \beta = \gamma = 90$ |
| Wavelength (Å) | 1.0000 |
| Resolution range (Å) | 50.00–2.70 (2.80–2.70) |
| Total reflections | 26984 |
| Unique reflections | 6807 |
| $R_{\rm merge}$† (%) | 4.8 (25.1) |
| Completeness (%) | 97.3 (83.1) |
| $\langle I/\sigma(I)\rangle$ | 17.3 (4.5) |
| Redundancy | 4.0 (3.1) |
| Crystal mosaicity (°) | 0.458 |

† $R_{\rm merge} = \sum_{hkl}\sum_i |I_i(hkl) - \langle I(hkl)\rangle| / \sum_{hkl}\sum_i I_i(hkl)$, where $I_i(hkl)$ is the $i$th intensity measurement of reflection $hkl$ and $\langle I(hkl)\rangle$ is its average.

ADSC Quantum 315 CCD detector installed on the BL41XU beamline at SPring-8. The data collection was performed at a wavelength of 1.000 Å over a total range of 180°, with individual frames of 1° and an exposure time of 4 s. The crystal-to-detector distance was 350 mm. The collected images were processed using *HKL*2000 (Otwinowski & Minor, 1997).

## 3. Results and discussion

CHP is an important regulatory factor that maintains the physiologically active conformation of NHE1. In this study, in order to clarify the regulatory mechanism of NHE1 by CHP, we coexpressed CHP2 and its binding domain in NHE1 (amino acids 503–545) in *E. coli* and crystallized the complex. Firstly, we confirmed that the purified complex CHP2–NHE1-peptide was retained as a single peak on gel-filtration chromatography, indicating that the stable complex exists as a monomer ($M_r$ = 28 000) in solution. In addition, using a 4–12% polyacrylamide gradient gel we confirmed that the purity of the complex is suitable for crystallization assay and that the purified sample contained equimolar amounts (1:1 molar ratio) of CHP2 and NHE1-peptide (Fig. 1).

Crystals suitable for X-ray crystallographic analysis were obtained within 2–3 d at 293 K using the sitting-drop vapour-diffusion method (Fig. 2). A previous attempt to collect crystallographic data at beamline BL44B2 (SPring-8) gave a maximum resolution of 3.0 Å owing to the small size of crystals. To obtain higher resolution data, we used the undulator beamline BL41XU. Crystals diffracted to 2.5 Å resolution along the $c$ axis of the crystal, but the data set was only qualitatively useful to 2.7 Å because of anisotropic diffraction.

The tetragonal crystal of CHP2–NHE1-peptide was determined to be $P4_1$ or $P4_3$, with unit-cell parameters $a = b = 49.96$, $c = 103.20$ Å. Assuming the presence of one CHP2–NHE1-peptide complex molecule in the asymmetric unit, the Matthews coefficient $V_{\rm M}$ was calculated to be 2.5 Å$^3$ Da$^{-1}$, indicating a solvent content of approximately 49.5% in the unit cell. These values are within the typical range for protein crystals (Matthews, 1968).

The native data set has 6807 unique reflections, giving a data-set completeness of 97.3% in the resolution range 50.0–2.7 Å, with an $R(I)_{\rm merge}$ of 4.8% (Table 1). Although CHP2 shows about 36% sequence identity with human CNB (PDB code 1aui; Kissinger *et al.*, 1995), molecular replacement using CNB as a search model with *MOLREP* (Vagin & Teplyakov, 1997) was unsuccessful. Further crystallization refinement and structural analysis by multi-wavelength anomalous dispersion methods using selenomethionine and also taking advantage of the presence of yttrium as an additive are in progress.

We thank the staff at beamlines BL44B2 and BL41XU, SPring-8 for data-collection support and Dr Tianxiang Pang for initial participation in this study. This work was supported by grant Nano-001 for Research on Advanced Medical Technology from the Ministry of Health, Labour and Welfare of Japan and Grant-in-Aid for Priority Areas 13142210 for Scientific Research from the Ministry of Education, Science and Culture of Japan. YBA was supported by a Japan Society for the Promotion of Science (JSPS) Postdoctoral Fellowship.

## References

Barroso, M. R., Bernd, K. K., DeWitt, N. D., Chang, A., Mills, K. & Sztul, E. S. (1996). *J. Biol. Chem.* **271**, 10183–10187.
Bertrand, B., Wakabayashi, S., Ikeda, T., Pouysségur, J. & Shigekawa, M. (1994). *J. Biol. Chem.* **269**, 13703–13709.
Counillon, L. & Pouysségur, J. (2000). *J. Biol. Chem.* **275**, 1–4.
Kissinger, C. R., Parge, H. E., Knighton, D. R., Lewis, C. T., Pelletier, L. A., Tempczyk, A., Kalish, V. J., Tucker, K. D., Showalter, R. E., Moomaw, E. W., Gastinel, L. N., Habuka, N., Chen, X., Maldonado, F., Barker, J. E., Bacquet, R. & Villafranca, J. E. (1995). *Nature (London)*, **378**, 641–644.
Lin, X. & Barber, D. L. (1996). *Proc. Natl Acad. Sci. USA*, **93**, 12631–12636.
Lin, X., Sikkink, R. A., Rusnak, F. & Barber, D. L. (1999). *J. Biol. Chem.* **274**, 36125–36131.
Matsumoto, M., Miyake, Y., Nagita, M., Inoue, H., Shitakubo, D., Takemoto, K., Ohtsuka, C., Murakami, H., Nakamura, N. & Kanazawa, H. (2001). *J. Biochem.* **130**, 217–225.
Matthews, B. W. (1968). *J. Mol. Biol.* **33**, 491–497.
Nakamura, N., Miyake, Y., Matsushita, M., Tanaka, S., Inoue, H. & Kanazawa, H. (2002). *J. Biochem.* **132**, 483–491.
Orlowski, J. & Grinstein, S. (2004). *Pflugers Arch.* **447**, 549–565.
Otwinowski, Z. & Minor, W. (1997). *Methods Enzymol.* **276**, 307–326.
Pang, T., Hisamitsu, T., Mori, H., Shigekawa, M. & Wakabayashi, S. (2004). *Biochemistry*, **43**, 3628–3636.
Pang, T., Su, X., Wakabayashi, S. & Shigekawa, M. (2001). *J. Biol. Chem.* **276**, 17367–17372.
Pang, T., Wakabayashi, S. & Shigekawa, M. (2002). *J. Biol. Chem.* **277**, 43771–43777.
Putney, L. K., Denker, S. P. & Barber, D. L. (2002). *Annu. Rev. Pharmacol. Toxicol.* **42**, 527–552.
Timm, S., Titus, B., Bernd, K. & Barroso, M. (1999). *Mol. Biol. Cell*, **10**, 3473–3488.
Vagin, A. A. & Teplyakov, A. (1997). *J. Appl. Cryst.* **30**, 1022–1025.
Wakabayashi, S., Bertrand, B., Ikeda, T., Pouysségur, J. & Shigekawa, M. (1994). *J. Biol. Chem.* **269**, 13710–13715.
Wakabayashi, S., Shigekawa, M. & Pouyssegur, J. (1997). *Physiol. Rev.* **77**, 51–74.

*Am J Physiol Heart Circ Physiol* 288: H1444–H1450, 2005.
First published November 11, 2004; doi:10.1152/ajpheart.00266.2004.

# Adrenomedullin enhances therapeutic potency of bone marrow transplantation for myocardial infarction in rats

Takafumi Fujii,[1] Noritoshi Nagaya,[2,3] Takashi Iwase,[2] Shinsuke Murakami,[2] Yoshinori Miyahara,[1] Kazuhiro Nishigami,[3] Hatsue Ishibashi-Ueda,[5] Mikiyasu Shirai,[1] Takefumi Itoh,[2] Kozo Ishino,[6] Shunji Sano,[6] Kenji Kangawa,[4] and Hidezo Mori[1]

*Departments of [1]Cardiac Physiology, [2]Regenerative Medicine and Tissue Engineering, [3]Internal Medicine, [4]Biochemistry, and [5]Pathology, National Cardiovascular Center, Osaka; and [6]Department of Cardiovascular Surgery, Okayama University Medical School, Okayama, Japan*

Submitted 18 March 2004; accepted in final form 19 October 2004

**Fujii, Takafumi, Noritoshi Nagaya, Takashi Iwase, Shinsuke Murakami, Yoshinori Miyahara, Kazuhiro Nishigami, Hatsue Ishibashi-Ueda, Mikiyasu Shirai, Takefumi Itoh, Kozo Ishino, Shunji Sano, Kenji Kangawa, and Hidezo Mori.** Adrenomedullin enhances therapeutic potency of bone marrow transplantation for myocardial infarction in rats. *Am J Physiol Heart Circ Physiol* 288: H1444–H1450, 2005. First published November 11, 2004; doi: 10.1152/ajpheart.00266.2004.—Adrenomedullin (AM), a potent vasodilator, induces angiogenesis and inhibits cell apoptosis through the phosphatidylinositol 3-kinase/Akt pathway. Transplantation of bone marrow-derived mononuclear cells (MNC) induces angiogenesis. We investigated whether infusion of AM enhances the therapeutic potency of MNC transplantation in a rat model of myocardial infarction. Immediately after coronary ligation, bone marrow-derived MNC ($5 \times 10^6$ cells) were injected into the ischemic myocardium, followed by subcutaneous administration of 0.05 $\mu g \cdot kg^{-1} \cdot min^{-1}$ AM (AM-MNC group) or saline (MNC group) for 3 days. Another two groups of rats received subcutaneous administration of AM alone (AM group) or saline (control group). Hemodynamic and histological analyses were performed 4 wk after treatment. Cardiac infarct size was significantly smaller in the MNC and AM groups than in the control group. A combination of AM infusion and MNC transplantation demonstrated a further decrease in infarct size. Left ventricular (LV) maximum change in pressure over time and LV fractional shortening were significantly improved only in the AM-MNC group. AM significantly increased capillary density in ischemic myocardium, suggesting the angiogenic potency of AM. AM infusion plus MNC transplantation demonstrated a further increase in capillary density compared with AM or MNC alone. Although MNC apoptosis was frequently observed 72 h after transplantation, AM markedly decreased the number of terminal deoxynucleotidyl transferase-mediated dUTP nick-end labeling-positive cells among the transplanted MNC. In conclusion, AM enhanced the angiogenic potency of MNC transplantation and improved cardiac function in rats with myocardial infarction. This beneficial effect may be mediated partly by the angiogenic property of AM itself and by its antiapoptotic effect on MNC.

angiogenesis; apoptosis; mononuclear cell

DESPITE THE RECENT REMARKABLE progress in medical and surgical treatment for ischemic heart disease, this disease remains a major cause of death worldwide (5). Bone marrow-derived mononuclear cells (MNC) contain various kinds of cell lineages and numerous cytokines that contribute to neovascularization (1, 15). In fact, autologous transplantation of bone marrow cells has been shown to enhance angiogenesis and improve cardiac function in an animal model of cardiac ischemia (6, 9, 10). Recent human studies have demonstrated beneficial effects of transplanted MNC in patients with ischemic heart disease (23, 25). However, some patients fail to respond to this cell therapy. Thus a novel therapeutic strategy to enhance the angiogenic property of MNC is desirable.

Adrenomedullin (AM) is a potent vasodilator peptide that was originally isolated from human pheochromocytoma (8). We have shown that infusion of AM has beneficial hemodynamic and renal effects in patients with heart failure (17). On the other hand, AM has been shown to activate the phosphatidylinositol 3-kinase (PI3-kinase)/Akt-dependent pathway in vascular endothelial cells, which is considered to regulate multiple critical steps in angiogenesis including endothelial cell proliferation, migration, and capillary-like formation (14, 22). In fact, we have shown that AM gene transfer induces therapeutic angiogenesis in a rabbit model of hindlimb ischemia via activation of Akt (24). These findings suggest that AM may play an important role in the regulation of vascular regeneration. In addition, AM has been shown to exert an antiapoptotic effect on a variety of cells including vascular endothelial cells (7, 20). Taking these findings together, combination therapy with MNC transplantation and AM infusion may have additional or synergetic effects on therapeutic angiogenesis for the treatment of ischemic heart disease.

Thus the purposes of this study were *1*) to investigate whether infusion of AM enhances the angiogenic potency of MNC transplantation in a rat model of myocardial infarction, and *2*) to investigate the effects of AM on survival and differentiation of the transplanted MNC to examine the underlying mechanisms of the effects induced by AM.

## MATERIALS AND METHODS

*Animal model.* Myocardial infarction was produced in male Lewis rats weighing 200–220 g by left coronary ligation. In brief, after rats were anesthetized by intraperitoneal injection of pentobarbital sodium (30 mg/kg body wt), they were ventilated artificially. The heart was exposed via left thoracotomy, and the left coronary artery was ligated 2–3 mm from its origin between the pulmonary artery conus and the left atrium using a 6-0 proline suture. Finally, the heart was restored to its normal position, and the chest was closed. The Animal Care Committee of the National Cardiovascular Center approved this experimental protocol.

Address for reprint requests and other correspondence: N. Nagaya, Dept. of Regenerative Medicine and Tissue Engineering, National Cardiovascular Center Research Institute, 5-7-1 Fujishirodai, Suita, Osaka 565-8565, Japan (E-mail: nnagaya@ri.ncvc.go.jp).

The costs of publication of this article were defrayed in part by the payment of page charges. The article must therefore be hereby marked "*advertisement*" in accordance with 18 U.S.C. Section 1734 solely to indicate this fact.

*Preparation of MNC.* After Lewis rats were killed, bone marrow from the femur and tibia was collected and put in PBS. Marrow cells were loaded on a 1.077 gradient of Ficoll (Lymphoprep; Nycomed Pharma, Oslo, Norway) and centrifuged at 1,500 rpm for 20 min. The cells were then washed with 10 ml PBS to remove the Ficoll and centrifuged at 2,000 rpm for 10 min. The cells were finally suspended in PBS at a concentration of $5 \times 10^6$ cells in 50 μl PBS for transplantation. Fluorescence-activated cell sorting analysis demonstrated that 22 ± 1% of MNC were positive for lectin from ulex europaeus (UEA)-1 lectin (Sigma, St. Louis, MO).

*MNC transplantation and AM infusion.* Transplantation of bone marrow-derived MNC and/or 3-day infusion of AM was performed immediately after coronary ligation. MNC ($5 \times 10^6$ cells in 50 μl PBS) were injected into the myocardium at five points in the border zone surrounding the infarct by using a 27-gauge needle. Recombinant human AM (0.05 $\mu g \cdot kg^{-1} \cdot min^{-1}$) was subcutaneously administered by using an osmotic minipump (model 2004; Alza, Palo Alto, CA) for 3 days. The pump was positioned in a pocket constructed in the subcutaneous tissue just below the subscapular region. For control, 5% glucose was infused in a similar manner in the rats receiving coronary ligation. This protocol resulted in the creation of four groups: *1*) AM infusion plus MNC transplantation (AM-MNC group, $n = 15$), *2*) vehicle infusion plus MNC transplantation (MNC group, $n = 14$), *3*) AM infusion plus PBS injection (AM group, $n = 14$), and *4*) vehicle infusion plus PBS injection (control group, $n = 13$).

*Echocardiographic studies.* Echocardiographic studies were performed 4 wk after surgery using a 7.5-MHz phased-array transducer (model HP SONOS 5500; Hewlett-Packard, Andover, MA). Rats were anesthetized by intraperitoneal injection of pentobarbital sodium (30 mg/kg body wt) as a supplement to maintain mild anesthesia. M-mode tracings were obtained at the level of the papillary muscles. Anterior and posterior end-diastolic wall thickness, left ventricular (LV) end-diastolic and end-systolic dimension, and LV fractional shortening were measured from three consecutive cardiac cycles by the American Society for Echocardiology leading-edge method (21).

*Cardiac catheterization.* Cardiac catheterization was performed 4 wk after surgery. Rats were anesthetized with intraperitoneal pentobarbital and placed on a heating pad to maintain body temperature at 37–38°C throughout the study. A 1.5 Fr micronanometer-tipped catheter was inserted in the right carotid artery for measurement of heart rate and mean arterial pressure. The catheter was then advanced into the LV for measurement of LV end-diastolic pressure and then replaced with a thermomicroprobe for measurements of cardiac output. These hemodynamic variables were measured with a pressure transducer (UFI, Morro Bay, CA) connected to a polygraph and recorded with a thermal recorder (model 7758 B system; Hewlett-Packard).

*Infarct size measurement.* After completion of hemodynamic measurements, the heart was arrested by an injection of 2 mmol KCl through the carotid artery, and the cardiac ventricles were excised. The size of myocardial infarction was determined by a previously described method (2). In brief, incisions were made in the LV so that the tissue could be pressed flat. The circumference of the entire flat LV and the visualized infarcted area, as judged from both the epicardial and endocardial sides, was outlined on a clear plastic sheet. The difference in weight between the two marked areas on the sheet was used to determine infarction size and was expressed as a percentage of LV surface area.

*Histological analysis of microvessel density.* LV myocardium was fixed in 10% formalin. Three cross sections of the LV, cut from apex to base, were obtained from individual rats for comparison among four groups ($n = 5$ each). They were embedded in paraffin and stained with Masson's trichrome for measurement of interstitial fibrosis. In other rats ($n = 5$ each), LV myocardium was embedded in optimum cutting temperature (OCT) compound (Sakura Finetechnical, Tokyo, Japan), snap frozen in liquid nitrogen, and cut into 5-μm-thick sections. Tissue sections were stained for alkaline phosphatase with an indoxyltetrazolium method to detect capillary endothelial cells ($n = 5$ in each group). The number of capillary vessels was counted in the peri-infarct area (a 1.0-mm band next to the scar) excluding scar region using a light microscope at a magnification of ×200. The numbers in five high-power fields in each rat were averaged and expressed as the number of capillary vessels. These morphometric studies were performed by two examiners who were blinded to treatment.

*Detection of MNC apoptosis.* To examine the antiapoptotic effect of AM on transplanted MNC, red fluorescence-labeled MNC were transplanted into ischemic myocardium in rats with ($n = 5$) and without ($n = 5$) AM infusion. Before implantation into the ischemic heart, suspended MNC were labeled with fluorescent dyes with a PKH26 (Red Fluorescent Cell Linker Kit; Sigma), as reported previously (13). AM was subcutaneously administered by using a minipump for 3 days. Rats were killed 72 h after MNC transplantation. The LV was enucleated, and muscle samples were embedded in OCT compound and snap frozen in liquid nitrogen for the detection of apoptosis. Serial sections of the heart were stained by terminal deoxynucleotidyl transferase-mediated dUTP nick-end labeling (TUNEL) for apoptosis using an in situ apoptosis detection kit (model S7111 Apoptag Fluorescein Kit; Intergen). Apoptosis of transplanted MNC was also evaluated by the detection of cleaved caspase-3-positive cells. In brief, the frozen tissue sections were incubated with anticleaved caspase-3 antibody (Cell Signaling), followed by incubation with FITC-conjugated IgG antibody (BD Pharmingen, San Diego, CA). The number of TUNEL/PKH26 double-positive cells and caspase-3/PKH26 double-positive cells was counted in 10 fields of each rat using a confocal microscopy (Fluoview model 500; Olympus, Tokyo, Japan).

The antiapoptotic effect of AM on MNC was also evaluated by in vitro TUNEL assay. MNC were plated on 12-well plates ($1 \times 10^6$ cells per well) and cultured in serum-free medium for 24 h with control buffer, AM ($1 \times 10^{-7}$ M), or AM plus wortmannin, a PI3-kinase inhibitor (50 nM). Randomly selected microscopic fields ($n = 10$) were evaluated for calculating the ratio of TUNEL-positive cells to total cells.

*Monitoring of implanted MNC in ischemic heart.* Additional rats were used to examine whether transplanted MNC differentiate into endothelial cells, cardiomyocytes, vascular smooth muscle cells, or macrophages in the ischemic heart. PKH26 (red fluorescence)-labeled MNC were injected into the ischemic heart in rats with ($n = 8$) and without ($n = 8$) AM infusion. These subgroups of rats were killed 4 wk after coronary ligation. To identify vascular endothelial cells in vivo, FITC-labeled UEA-1 lectin was intravenously administered 30 min before the rats were killed ($n = 5$ in each group). The LV was enucleated, and muscle samples were then embedded in OCT compound, snap frozen in liquid nitrogen, and cut into sections. Sections were counterstained with 4′,6′-diamidino-2-phenylindole (DAPI) to detect nuclei. The number of DAPI/PKH26 double-positive cells and lectin-positive cells in the peri-infarct area was counted in 10 fields of each rat using a confocal microscopy. Frozen sections from other rats ($n = 3$ in each group) were incubated with mouse anticardiac troponin T (Novocastra, Newcastle, UK), anti-α-smooth muscle actin antibody (Dako, Copenhagen, Denmark), and anti-ED1 antibody (Serotec, Oxford, UK), followed by incubation with FITC-conjugated IgG antibody. In other rats (MNC group, $n = 5$; AM-MNC group, $n = 5$), the cardiac muscle from base to apex was transversely cut into 6-μm slices to calculate the number of transplanted MNC present within the heart 4 wk after transplantation. These morphometric studies were performed by two examiners who were blinded to treatment.

*Statistical analysis.* Numerical values were expressed as means ± SE. Comparisons of parameters among the four groups were performed by one-way ANOVA, followed by Newman-Keuls test for unpaired data. Comparisons of parameters between two groups were made by unpaired Student's *t*-test. A value of $P < 0.05$ was considered significant.

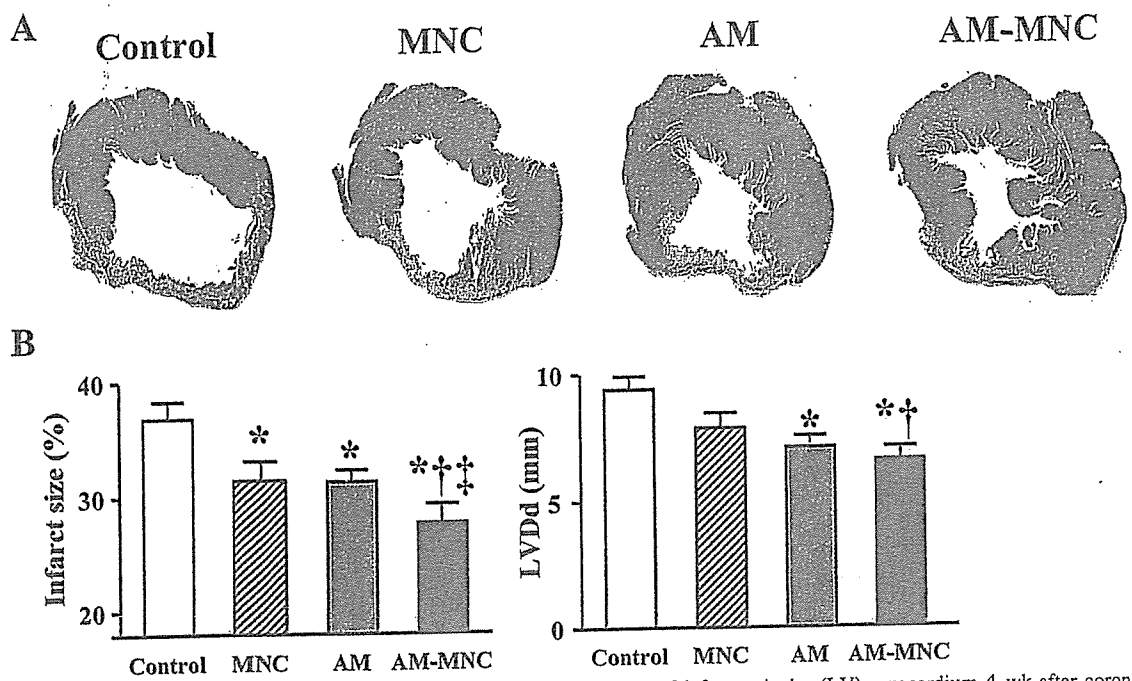


Fig. 1. *A*: representative examples of Masson trichrome-staining of transverse sections of left ventricular (LV) myocardium 4 wk after coronary ligation. *B*: quantitative analysis of infarct size and LV chamber size. Infarcted area and LV end-diastolic diameter (LVDd) of the adrenomedullin-mononuclear cell (AM-MNC) group were significantly smaller than those of the other groups. Values are means ± SE. *$P < 0.05$ vs. control; †$P < 0.05$ vs. MNC; ‡$P < 0.05$ vs. AM.

## RESULTS

*Infarct size and ventricular weight.* Moderate-to-large infarcts were observed in the control group after coronary ligation (Fig. 1). However, infarct size was smaller in the MNC, AM, and AM-MNC groups than in the control group. In particular, it was very small in the AM-MNC group. Quantitative analysis also demonstrated that cardiac infarct size in the AM-MNC group was smallest among the four groups. Right ventricular weight was significantly lower in the AM and AM-MNC groups than that in the control group (Table 1). LV weight did not significantly differ among the four groups.

*Echocardiographic findings.* LV diastolic dimension was smallest in the AM-MNC group, followed by the AM, MNC, and control groups (Fig. 1). LV fractional shortening in the AM-MNC group was also higher than that in the control, MNC, and AM groups (Table 2). Diastolic thickness of the anterior wall was significantly attenuated in the MNC, AM, and AM-MNC groups compared with the control group.

*Hemodynamics.* Cardiac output in the AM-MNC group was significantly higher than that in the control, MNC, and AM groups (Fig. 2). LV end-diastolic pressure in the MNC, AM, and AM-MNC groups was significantly lower than that in the control group. LV maximum change in pressure over time ($dP/dt$) in the MNC and AM-MNC group were significantly higher than that in the control group. Similarly, LV minimum $dP/dt$ was significantly decreased only in the AM-MNC group.

*Capillary density.* Alkaline phosphatase staining of ischemic myocardium showed marked augmentation of neovascularization in the MNC, AM, and AM-MNC groups compared with the control group (Fig. 3*A*). Quantitative analysis demonstrated that capillary density was significantly higher in the AM-MNC group than in the MNC and AM groups (Fig. 3*B*). Cartilage, bone, or fat was not observed in the transplanted area. No tumor-like cells were seen.

*Antiapoptotic effect of AM on MNC.* Red fluorescence-labeled MNC were detected in each recipient heart 72 h after transplantation (Fig. 4). TUNEL-positive cells were frequently observed in the MNC group. In contrast, these apoptotic cells

Table 1. *Physiological profiles of four experimental groups*

| | Control | MNC | AM | AM-MNC |
|---|---|---|---|---|
| Number | 13 | 14 | 14 | 15 |
| Body weight, g | 274±3 | 285±5 | 287±3 | 305±4* |
| Heart rate, bpm | 410±24 | 404±30 | 398±33 | 387±36 |
| MAP, mmHg | 101±11 | 104±13 | 103±9 | 116±14* |
| LV wt/body wt, g/kg | 2.4±0.2 | 2.5±0.2 | 2.6±0.1 | 2.5±0.2 |
| RV wt/body wt, g/kg | 1.1±0.1 | 0.9±0.1 | 0.8±0.1* | 0.7±0.1* |

Values are means ± SE; number is number of rats in each group. Control group, myocardial infarction rats given vehicle; MNC group, those given mononuclear cells; AM, those given adrenomedullin; AM-MNC, those given AM and MNC; MAP, mean arterial pressure; LV, left ventricle; RV, right ventricle. *$P < 0.05$ vs. control.

Table 2. *Echocardiographic findings*

| | Control | MNC | AM | AM-MNC |
|---|---|---|---|---|
| LVDd, mm | 9.9±0.2 | 8.3±0.3 | 7.3±0.2* | 6.9±0.3*† |
| LVDs, mm | 8.4±0.3 | 6.6±0.4 | 5.8±0.2* | 5.1±0.2* |
| %FS, % | 14±1 | 22±1* | 21±1* | 26±1*†‡ |
| AWT diastole, mm | 1.0±0.2 | 1.3±0.3* | 1.3±0.3* | 1.4±0.4* |
| PWT diastole, mm | 1.5±0.5 | 2.2±0.4 | 2.1±0.4 | 2.2±0.4 |

Values are means ± SE. LVDd, LV diastolic dimension; LVDs, LV systolic dimension; %FS, LV fractional shortening; AWT, anterior wall thickness; PWT, posterior wall thickness. *$P < 0.05$ vs. control; †$P < 0.05$ vs. MNC; ‡$P < 0.05$ vs. AM.

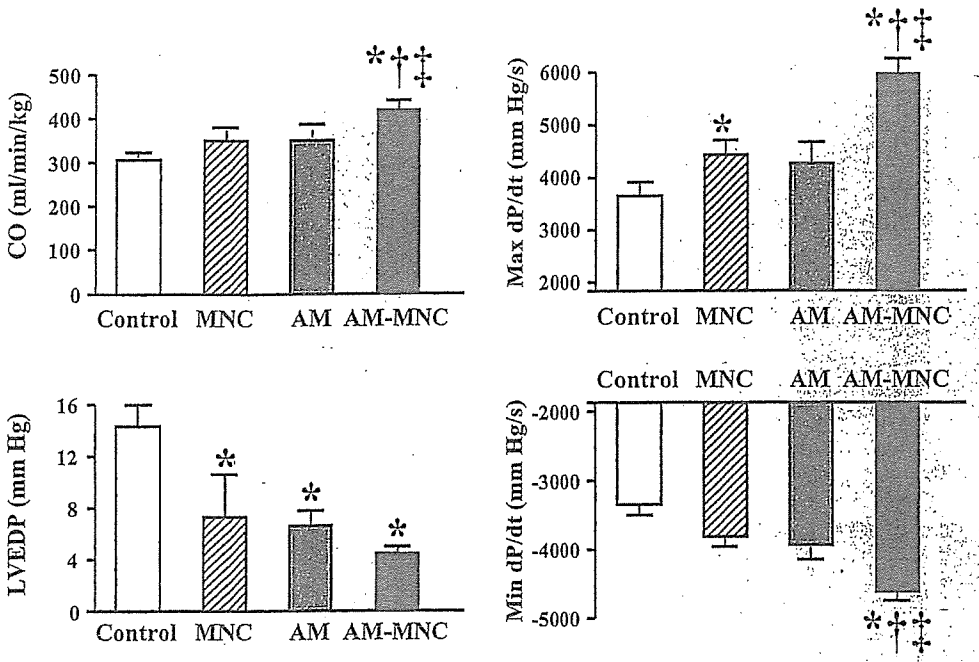


Fig. 2. Effects of AM infusion and MNC transplantation on hemodynamic parameters. CO, cardiac output; LVEDP, LV end-diastolic pressure; Max dP/d*t*, LV maximum change in pressure over time; Min dP/d*t*, LV minimum dP/d*t*. Values are means ± SE. *$P < 0.05$ vs. control; †$P < 0.05$ vs. MNC; ‡$P < 0.05$ vs. AM.

were hardly detected in the AM-MNC group. Semiquantitative analysis demonstrated that the number of TUNEL-positive MNC was significantly lower in the AM-MNC group than in the MNC group. Similarly, the number of caspase-3-positive MNC was significantly lower in the AM-MNC group than in the MNC group. These results suggest that infusion of AM inhibits apoptosis of transplanted MNC.

In vitro, serum starvation induced MNC apoptosis. When incubated in the presence of AM ($1 \times 10^{-7}$ M), the percentage of TUNEL-positive cells decreased significantly (19 ± 1 to 9 ± 1%, $P < 0.05$). However, pretreatment with wortmannin, a PI3-kinase inhibitor, diminished the antiapoptotic effect of AM (17 ± 1%).

*Differentiation of MNC into endothelial lineage.* Four weeks after transplantation, fluorescence-labeled transplanted cells

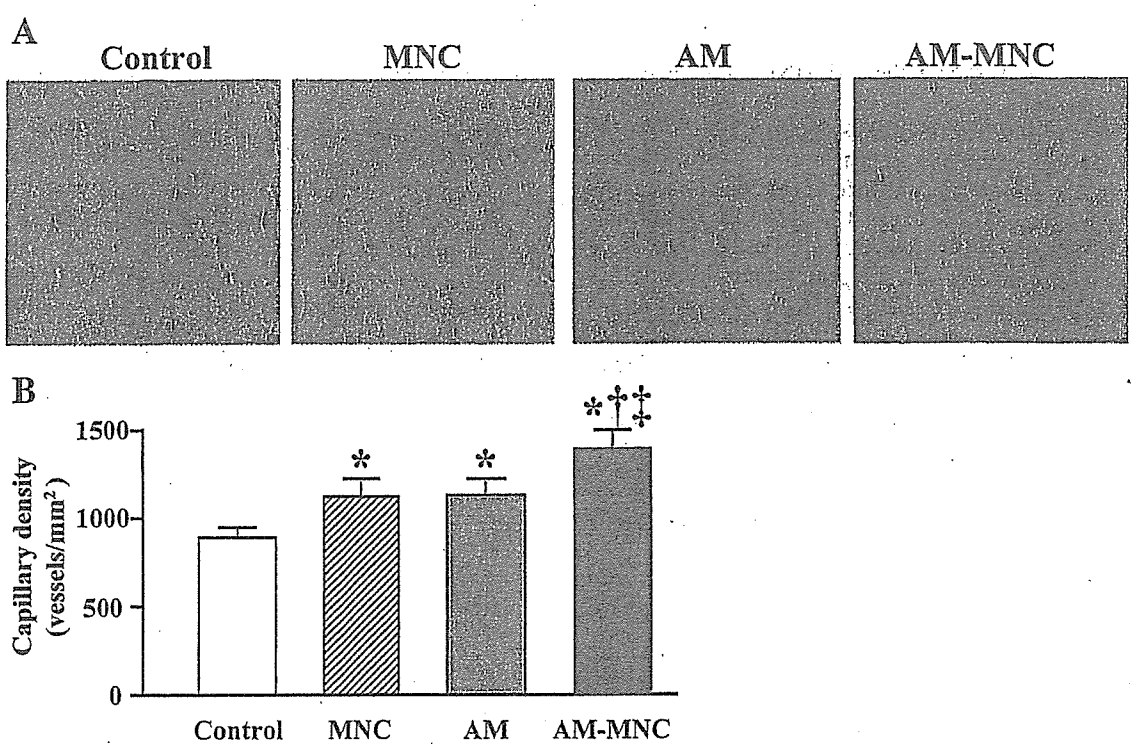


Fig. 3. *A*: representative examples of alkaline phosphatase staining in peri-infarct area. A combination of AM infusion and MNC transplantation markedly induced myocardial neovascularization. Magnification, ×200. *B*: quantitative analysis of capillary density in peri-infarct area. Capillary density in the AM-MNC group was significantly higher than that in the MNC and AM groups. Values are means ± SE. *$P < 0.05$ vs. control; †$P < 0.05$ vs. MNC; ‡$P < 0.05$ vs. AM.

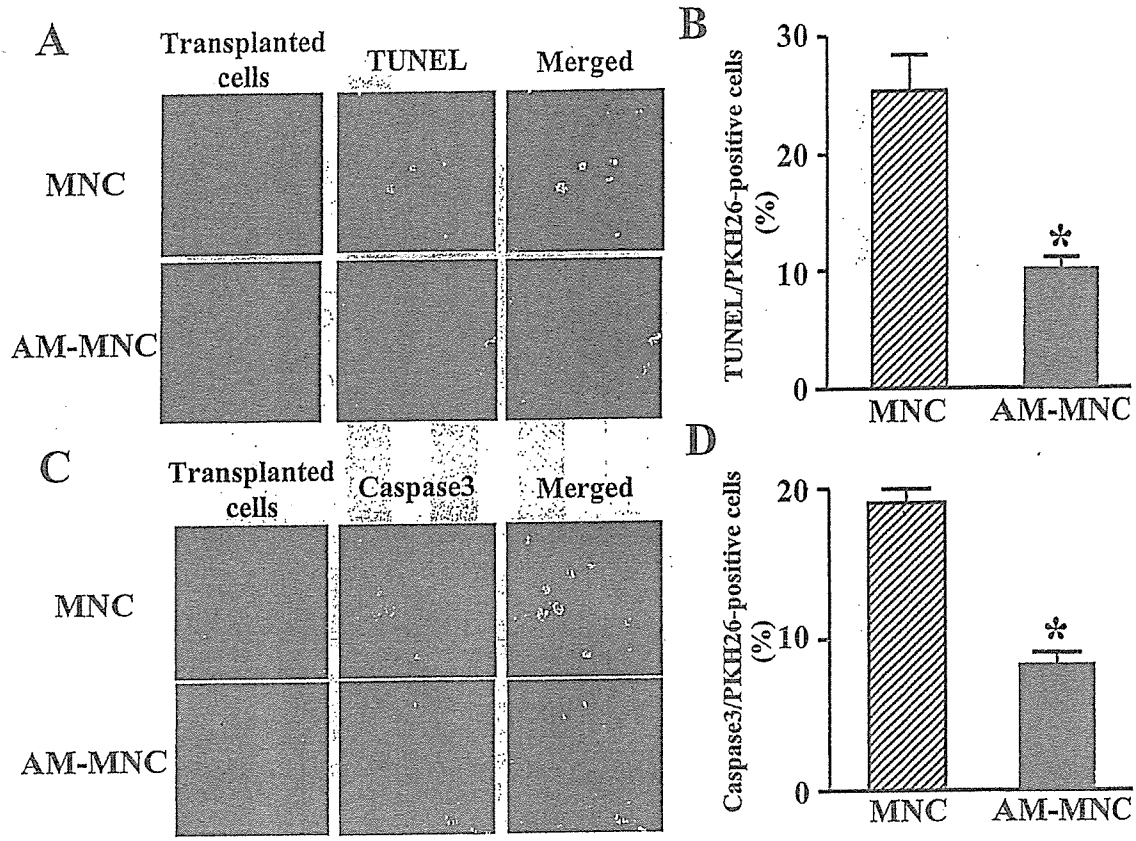


Fig. 4. Detection of transplanted cell apoptosis. *A*: representative photographs of terminal deoxynucleotidyl transferase-mediated dUTP nick end labeling (TUNEL) staining. Red fluorescence (PKH26) marks transplanted MNC; green fluorescence indicates TUNEL-positive cells. TUNEL-positive cells were frequently observed in the MNC group, whereas they were hardly detected in the AM-MNC group. Magnification, ×400. *B*: semiquantitative analysis of TUNEL-positive cells in the PKH26-positive (transplanted) cells. *C*: representative photographs of caspase-3 staining. Red fluorescence (PKH26) marks transplanted MNC; green fluorescence indicates caspase-3-positive cells. *D*: semiquantitative analysis of caspase-3-positive cells in the PKH26-positive cells. Values are means ± SE. $*P < 0.05$ vs. control.

were more frequently observed in the AM-MNC group than in the MNC group (6.4 ± 0.4 to 3.1 ± 0.2%, $P < 0.05$). Moreover, some of the transplanted cells were positive for UEA-1 lectin in the AM-MNC group (Fig. 5*A*), suggesting differentiation of MNC into vascular endothelial cells. Semiquantitative analysis demonstrated that the number of DAPI/PKH26 double-positive cells (viable transplanted cells) was significantly higher in the AM-MNC group than in the MNC group (Fig. 5*B*). Moreover, the ratio of lectin-positive cells to DAPI/PKH26 double-positive cells was significantly higher in the AM-MNC group than in the MNC group. The ratio of DAPI/PKH26 double-positive cells to lectin-positive cells was small, but significantly higher in the AM-MNC group than in the MNC group (23.9 ± 0.9 to 17.2 ± 0.6%, $P < 0.01$). Transplanted MNC were negative for troponin T or α-smooth muscle actin-positive cells. Some of the transplanted MNC were positive for ED1, a marker of macrophage (data not shown).

## DISCUSSION

In the present study, we demonstrated that *1*) infusion of AM enhanced the angiogenic potency of MNC in a rat model of acute myocardial infarction, resulting in decreased infarct size and improved cardiac function. We also demonstrated that *2*) AM induced angiogenesis and inhibited apoptosis of the transplanted MNC. Thus a combination of AM and MNC may have beneficial effects in rats with myocardial infarction, partly through the angiogenic potency of AM itself and through its antiapoptotic effect on MNC.

Bone marrow-derived MNC include a variety of stem and progenitor cells (1, 15, 19), some of which can differentiate into endothelial cells and secrete numerous cytokines and chemokines (6, 9, 10). Earlier studies (6, 9, 10, 23, 25) have shown that autologous bone marrow transplantation induces angiogenesis and improves LV function in animals and humans. However, some patients are refractory to this cell therapy. Thus an approach to augment the angiogenic potency of MNC transplantation is required.

The present study showed that MNC transplantation or AM infusion alone reduced infarct size. A combination of AM infusion and MNC transplantation resulted in further decreases in infarct size and LV chamber size. MNC transplantation or AM administration modestly improved LV function. On the other hand, a combination of MNC and AM significantly improved cardiac performance compared with MNC or AM alone, as indicated by increases in cardiac output, fractional shortening, and LV maximum $dP/dt$. Earlier studies (6, 9, 10) have reported that MNC transplantation induces therapeutic angiogenesis and preserves LV function through inhibition of cardiomyocyte apoptosis in animal models of myocardial infarction. We have shown that AM infusion during the acute phase of ischemia-reperfusion inhibits apoptosis of cardiomyocytes and produces hemodynamic improvement in an animal

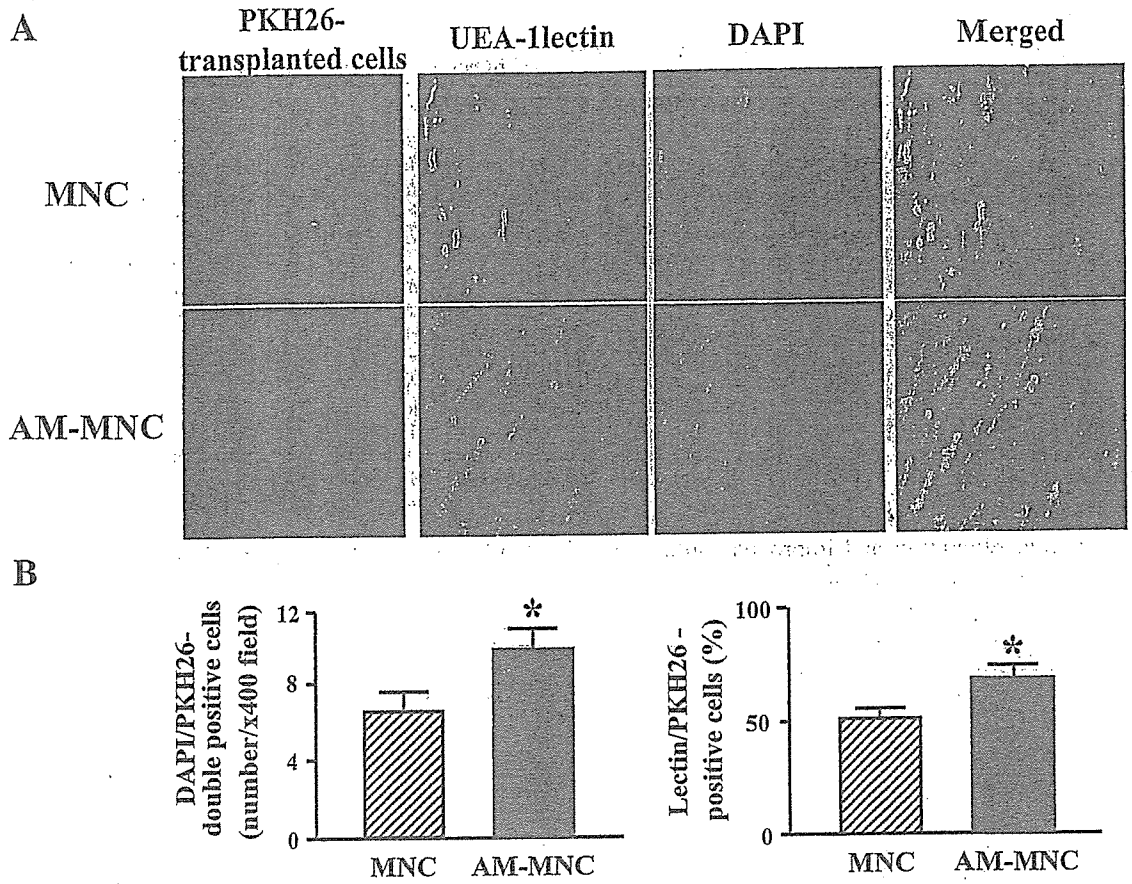


Fig. 5. *A*: representative examples of MNC differentiation into endothelial lineage. Red fluorescence (PKH26) marks transplanted cells; green fluorescence indicates ulex europaeus (UEA)-1 lectin, a marker for vascular endothelial cells. Most of the transplanted cells differentiated into endothelial cells in the AM-MNC group. Magnification, ×400. *B*: quantitative analysis of living transplanted cells and endothelial differentiation. The number of living cells after transplantation was significantly higher in the AM-MNC group than in the MNC group. The ratio of lectin-positive cells to living transplanted cells was significantly higher in the AM-MNC group than in the MNC group. Values are means ± SE. $*P < 0.05$ vs. control. DAPI, 4′,6′-diamidino-2-phenylindole.

study (18). These findings suggest that the reduction of infarct size induced by this combination therapy may be attributable to additive cardioprotective effects of MNC and AM.

The present study showed that AM infusion significantly increased capillary density in ischemic myocardium. Furthermore, AM infusion plus MNC transplantation demonstrated a further increase in capillary density compared with AM or MNC alone. Contribution of transplanted MNC to neovascularization (the ratio of DAPI/PKH26 double-positive cells to lectin-positive cells) was significantly greater in the AM-MNC group than in the MNC group. A recent study (14) has reported that AM promotes proliferation and migration of human umbilical vein endothelial cells and enhances angiogenesis in a murine gel plug assay through the PI3-kinase/Akt pathway. We have also shown that intramuscular administration of AM DNA induces therapeutic angiogenesis in a rabbit model of chronic hindlimb ischemia via activation of Akt (24). These findings suggest that the beneficial effects of combination therapy using AM and MNC may be attributable, in part, to the angiogenic properties of AM itself. Thus it is possible that AM infusion and MNC transplantation induce additive effects on myocardial damage after myocardial infarction. However, it still remains unknown whether AM infusion plus MNC transplantation induces synergetic effects.

An earlier study has demonstrated that ischemia and mechanical stress induce apoptosis of transplanted cells in the early stage after MNC transplantation (9). These results raise the possibility that the angiogenic potency of MNC transplantation is attenuated by MNC apoptosis. Kim et al. (7) have demonstrated that AM inhibits apoptosis of endothelial cells through the PI3-kinase/Akt pathway in vitro. Activation of the PI3-kinase/Akt pathway has been shown to inhibit apoptosis of endothelial progenitor cells and enhance neovascularization (11). In the present study, AM infusion significantly inhibited MNC apoptosis in ischemic tissue. In vitro, we showed that the antiapoptotic effect of AM on MNC was mediated by activation of the PI3-kinase/Akt pathway. Thus AM may enhance the therapeutic potency of MNC transplantation through a direct action of AM on MNC survival. Moreover, immunohistological examination demonstrated that infusion of AM increased the number of lectin-positive (endothelial) cells in transplanted MNC. These findings raise the possibility that AM may enhance differentiation of MNC into the endothelial lineage. Thus AM may directly act on transplanted MNC, which may result in synergetic effects on the ischemic myocardium.

This study includes some study limitations. Although the labeling efficacy of PKH26 has been shown to persist for >8 wk without cell toxicity (3, 4), the used vital marker PKH26